


AUTHOR QUERY FORM

 ELSEVIER	Journal: APNUM Article Number: 3378	Please e-mail your responses and any corrections to: E-mail: corrections.esch@elsevier.vtex.it
--	--	--

Dear Author,

Please check your proof carefully and mark all corrections at the appropriate place in the proof. **It is crucial that you NOT make direct edits to the PDF using the editing tools as doing so could lead us to overlook your desired changes.** Rather, please request corrections by using the tools in the Comment pane to annotate the PDF and call out the changes you would like to see. To ensure fast publication of your paper please return your corrections within 48 hours.

For correction or revision of any artwork, please consult <http://www.elsevier.com/artworkinstructions>

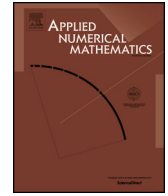
Any queries or remarks that have arisen during the processing of your manuscript are listed below and highlighted by flags in the proof.

Location in article	Query / Remark: Click on the Q link to find the query's location in text Please insert your reply or correction at the corresponding line in the proof
Q1	Your article is registered as a regular item and is being processed for inclusion in a regular issue of the journal. If this is NOT correct and your article belongs to a Special Issue/Collection please contact <t.gunasekaran.1@elsevier.com> immediately prior to returning your corrections. (p. 1/ line 1)
Q2	The author names have been tagged as given names and surnames (surnames are highlighted in teal color). Please confirm if they have been identified correctly and are presented in the desired order. (p. 1/ line 15)
Q3	Please note that the reference style has been changed from a Name-Year style to a Numbered style as per the journal specifications. (p. 2/ line 9)
Q4	Figure(s) will appear in black and white in print and in color on the web. The figure(s) contains references to color or the colors are mentioned in the main text. Based on this, the explanatory text about the interpretation of the colors has been added. Please check, and correct if necessary. (p. 3/ line 15)
Q5	Please check if sponsor name has been identified correctly and correct if necessary. (p. 21/ line 5)
	<div data-bbox="566 1669 1110 1790"> Please check this box or indicate your approval if you have no corrections to make to the PDF file <input data-bbox="1010 1695 1087 1759" type="checkbox"/> </div>



Contents lists available at ScienceDirect

Applied Numerical Mathematics

www.elsevier.com/locate/apnum

Smooth subgrid fields underpin rigorous closure in spatial discretisation of reaction–advection–diffusion PDEs

G.A. Jarrad^a, A.J. Roberts^{b,*}^a University of Adelaide, South Australia 5000, Australia^b School of Mathematical Sciences, University of Adelaide, South Australia 5005, Australia

ARTICLE INFO

Article history:

Received 8 December 2017

Received in revised form 3 May 2018

Accepted 21 May 2018

Available online xxxx

Keywords:

Spatial discretization

Rigorous closure

Partial differential equation

Centre manifold

Inter-element coupling

ABSTRACT

Finite difference/element/volume methods of spatially discretising PDEs impose a subgrid scale interpolation on the dynamics. In contrast, the so-called holistic discretisation approach developed herein constructs a natural subgrid scale field adapted to the whole system out-of-equilibrium dynamics. Consequently, the macroscale discretisation is systematically informed by the underlying microscale dynamics. We establish a new proof that there exists an exact closure of the spatially-discrete dynamics of a general class of reaction–advection–diffusion PDEs. The approach also constructs new systematic approximations to the in-principle closure starting from a basis of simple, piecewise-linear, continuous approximation. Under inter-element coupling conditions that guarantee continuity of several field properties, the constructed holistic discretisation possesses desirable properties such as a natural cubic spline first-order approximation to the field, and the self-adjointness of the diffusion operator under periodic, Dirichlet and Neumann macroscale boundary conditions. As a concrete example, we demonstrate the holistic discretisation procedure on the well-known Burgers' PDE, and compare the theoretical and numerical stability of the resulting discretisation to other approximations. The approach developed here promises to empower systematic construction of good, macroscale discretisations to a wide range of dissipative and wave PDEs.

© 2018 Published by Elsevier B.V. on behalf of IMACS.

1. Introduction

We explore accurate and stable spatial discretisations of nonlinear PDEs for a field $u(x, t)$ satisfying non-autonomous reaction–advection–diffusion PDEs in the general form

$$u_t = F(u_x)_x + \alpha G(x, t, u, u_x) \quad (1)$$

for suitably smooth functions F and G , and F strictly monotonic increasing, where subscripts x and t denote spatial and temporal derivatives, respectively. Precise requirements on the class of functions F and G are identified in Theorem 6 (§3). Although most of this article addresses PDEs of the form (1), Section 3.1 discusses generalising the theoretical support to wave-like PDEs obtained by replacing u_t by u_{tt} in (1).

* Corresponding author.

E-mail addresses: Geoff.jarrad@gmail.com (G.A. Jarrad), anthony.roberts@adelaide.edu.au (A.J. Roberts).

<https://doi.org/10.1016/j.apnum.2018.05.011>

0168-9274/© 2018 Published by Elsevier B.V. on behalf of IMACS.

Given $N + 1$ discrete points in 1D space, $x = X_j$ for $j \in \mathbb{J} = \{0, 1, \dots, N\}$, we define grid values

$$U_j(t) := u(X_j, t) \quad \text{for all } j \in \mathbb{J}, t \in \mathbb{T}. \quad (2)$$

Then a spatial discretisation of the PDE (1) is a closed set of ODEs for $\vec{U} = (U_0, \dots, U_N)$ in the form

$$\frac{d\vec{U}}{dt} = \vec{g}(\vec{U}, t). \quad (3)$$

We use centre manifold theory (e.g. [5,11]) to do the following (Section 3): firstly, establish a new approach to showing that in principle there exists an exact closure (3) of the dynamics of the PDE (1) in some \vec{U} -domain; secondly, establish that such a closure is emergent from general initial conditions; and thirdly, show how to construct new systematic approximations to the in-principle closure. This new theory is applied in Sections 4 and 4.2 to construct and evaluate the new approach for the classic example of the nonlinear advection–diffusion Burgers' PDE

$$\frac{\partial u}{\partial t} = \nu \frac{\partial^2 u}{\partial x^2} - \alpha u \frac{\partial u}{\partial x}, \quad (4)$$

for both diffusion ν and nonlinearity parameter α being real and constant. This PDE is commonly used as a first test of such discretisation schemes (e.g. [8]). Generalisation of the approach to two or more spatial dimensions remains for further research and should be analogous to that established by Roberts et al. [27].

Initial conditions for the discrete closure (3) are nontrivial. The paradox is that despite the definition (2) that $U_j(t) = u(X_j, t)$, in general the initial grid value $U_j(0) \neq u(X_j, 0)$ for accurate forecasts over long-times. In physics, van Kampen [30] called this phenomena “initial slip”, and it is effectively a ‘boundary layer’ in time that accounts for rapid transients. Roberts [19] developed an efficient general method that would algebraically derive the correct initial $U_j(0)$ for accurate long-time forecasts—the method has been successful in various other applications (e.g. [24]).

The spatial domain \mathbb{X} of the PDE (1) is of length L , $0 \leq x \leq L$, and we mostly restrict attention to solutions $u(x, t)$ which are L -periodic in space, but occasionally comment on the cases of homogeneous Dirichlet boundary conditions, $u(0, t) = u(L, t) = 0$, and Neumann boundary conditions, $u_x(0, t) = u_x(L, t) = 0$. The first step is to partition \mathbb{X} into N equi-spaced intervals bounded by the $N + 1$ grid-points X_j with spacing H . Traditional spatial discretisation of such PDEs, whether finite difference, finite element, or finite volume, imposes assumed fields in each element and then derives approximate rules for the evolution in time of the parameters of the imposed fit. Our dynamical systems (holistic) approach is to let the PDE (1) determine the subgrid fields in order to remain faithful to the PDE, as demonstrated explicitly for Burgers' PDE (4). Using more general subgrid scale structures is cognate to the aims of the so-called Generalised/Extended Finite Element Methods (e.g. [29]), but a crucial distinction is that we let the PDE determine the subgrid structures. The multiscale derivation of the so-called stabilized schemes (e.g. [12]) appears analogous to the first step of the construction described by Section 4. A previous dynamical systems approach constructs subgrid fields by systematically refining a piecewise constant initial approximation (e.g. [21,22,27])—an approach that adapts to the multi-scale gap-tooth scheme (e.g. [26,14]). The new approach here systematically refines a continuous piecewise linear initial approximation with the aim of more accurately encoding subgrid scale effects in the macroscale closure.

New theory established in Section 3 asserts that in principle an exact closure (3) exists (a slow manifold); that is, there is some system of ODEs (3) that gives exact solutions of the PDE (1). A traditional approach is to use centred approximations: for the example of Burgers' PDE (4),

$$\begin{aligned} \dot{U}_j &\approx -\alpha \frac{1}{2H} U_j (U_{j+1} - U_{j-1}) + \nu \frac{1}{H^2} (U_{j+1} - 2U_j + U_{j-1}) \\ &= -\alpha U_j \mu \delta U_j / H + \nu \delta^2 U_j / H^2, \end{aligned}$$

for centred difference $\delta := \sigma^{1/2} - \sigma^{-1/2}$, and centred mean $\mu := (\sigma^{1/2} + \sigma^{-1/2})/2$, in terms of the shift operator $\sigma U_j = U_{j+1}$. However, the nonlinear advection term has another plausible representation, namely the conservative form $\mu \delta(U_j^2)/2H$. For illustrative purposes, Section 4 compares results with Burgers' PDE (4) on a periodic domain discretised to the so-called mixture model

$$\dot{U}_j = -(1 - \theta) \alpha \frac{U_j \mu \delta U_j}{H} - \theta \alpha \frac{\mu \delta(U_j^2)}{2H} + \nu \frac{\delta^2 U_j}{H^2}, \quad (5)$$

for N -periodic index j . In contrast, Section 4 shows our holistic approach has no such representational ambiguity, and constructs at first-order the specific model

$$\dot{U}_j = S \left[-\alpha \frac{U_j \mu \delta U_j}{3H} - \alpha \frac{\mu \delta(U_j^2)}{3H} + \nu \frac{\delta^2 U_j}{H^2} \right], \quad (6)$$

for nonlocal operator $S = (1 + \delta^2/6)^{-1}$. Apart from the operator S , this holistic model matches the mixture model (5) for parameter $\theta = \frac{2}{3}$. This parameter value is exactly the critical value shown by [17] to be necessary for stable simulation (with

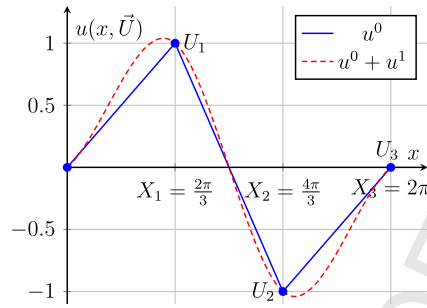


Fig. 1. An example of the smooth subgrid field provided by the holistic discretisation process, where the piecewise-linear initial approximation $u^0(x, \vec{U})$ is smoothed by the first-order correction $u^1(x, \vec{U})$ (for nonlinearity $\alpha = 0$). The correction u^1 forms a cubic spline; however, it is derived directly from the PDE itself, rather than obtained by imposing such an interpolation. (For interpretation of the colours in the figure(s), the reader is referred to the web version of this article.)

$\nu = 0$ and $\alpha = 1$) for a selection of numerical integration schemes. Section 4.2 further compares the numerical behaviour of our holistic and established mixture models.

A crucial part of the new methodology is to express the physical field $u(x, t)$ naturally in terms of the coarse variables $\vec{U}(t)$ for out-of-equilibrium dynamics. That is, as illustrated by the two approximate examples of Fig. 1, we construct the field (a slow manifold)

$$u(x, t) = u(x, t, \vec{U}(t)), \quad (7)$$

where the time evolution of the field u occurs only via the evolving coarse variables $\vec{U}(t)$ and any time dependent coefficients of the PDE. Whether the symbol u denotes $u(x, t)$ or $u(x, t, \vec{U})$ should be clear from the context. The complete holistic framework comprises equations (3) and (7), in conjunction with suitable boundary and inter-element coupling conditions to be specified in more detail in Section 3.

In particular, the Rayleigh–Ritz theorem motivates coupling conditions that give a piecewise linear function as the leading approximation (the blue u^0 of Fig. 1). Approximately constructing a slow manifold is analogous to estimating eigenvalues of a periodic matrix. For a self-adjoint operator \mathcal{L} , the Rayleigh–Ritz theorem is that an approximate eigenvector \vec{v} , with error $\|\vec{v} - \vec{v}_i\|$, predicts a corresponding eigenvalue $\lambda = \langle \vec{v}, \mathcal{L}\vec{v} \rangle / \|\vec{v}\|^2$ with asymptotically smaller error $\mathcal{O}(\epsilon^2)$. This suggests that the more accurate we make an initial approximation to the field u , the more accurate the predicted evolution on the slow manifold. Consequently, this article develops a systematic approximation to an in-principle exact discrete closure based upon the novel approach of using centre manifold techniques to systematically refine a piecewise linear and continuous subspace approximation to the field u .

2. An example introduces theory and method

As an introduction to the methodology, theory and results, this section investigates the modelling of Burgers' PDE (4) on the specific domain $-1 < x < 1$, with basic Dirichlet boundary conditions that $u(\pm 1, t) = 0$, and with viscosity $\nu = 1$ for definiteness. For introductory simplicity, the domain space is partitioned into just two intervals, $-1 < x < 0$ and $0 < x < 1$. Our aim is to model the dynamics of the whole field $u(x, t)$ by simply the dynamics of the grid value $U(t) := u(0, t)$ of the field at the single, central, interior grid-point $X = 0$.

The dynamics in the two intervals need to be coupled to each other to form a solution valid over the whole domain. Conventional numerical methods impose an assumed interpolation field and then derive a corresponding model. In contrast, here we craft a coupling that moderates the communication between the two intervals, and then let the PDE (4) itself tell us the appropriate out-of-equilibrium fields and model. The desired full coupling between the two intervals is of C^1 continuity: $[u] = [u_x] = 0$ where we introduce $[\cdot]$ to denote the jump in value across the grid-point $X = 0$; that is, $[u] = u|_{0+} - u|_{0-}$. For reasons developed below, we embed Burgers' PDE (4) in a family of problems with the moderated coupling between intervals of

$$[u] = 0 \quad \text{and} \quad [u_x] + 2(1 - \gamma)u = 0 \quad \text{at } x = X = 0; \quad (8)$$

that is, the field is continuous but the derivative has a discontinuity depending upon homotopy parameter γ (corresponding to the general case (13)). We derive below that $\gamma = 0$ provides a useful base to apply powerful centre manifold theory. When $\gamma = 1$, the coupling (8) requires C^1 continuity across $x = 0$ to restore the PDE over the entire spatial domain.

To show there is a useful (slow) centre manifold, we start with equilibria in the system (corresponding to Lemma 1 on p. 6). The PDE (4), with diffusivity $\nu = 1$, together with coupling conditions (8), and the Dirichlet boundary conditions, has a subspace \mathbb{E} of equilibria parametrised by U :

$$u = (1 - |x|)U \quad \text{and} \quad \gamma = \alpha = 0. \quad (9)$$

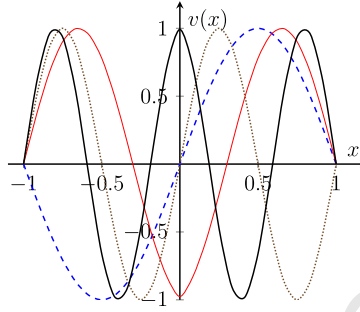


Fig. 2. Eigenfunctions $v(x)$ of the linearised problem (10) corresponding to negative eigenvalues: blue-dashed, $-\pi^2$; red-thin, -20.191 ; brown-dotted, $-4\pi^2$; and black-thick, -59.680 .

The spectrum about each of these equilibria determine the manifold structure (corresponding to Lemmas 3 and 4 on pp. 8, 9). We seek linearised solutions $u(x, t) \approx (1 - |x|)U + e^{\lambda t}v(x)$ for small v : the diffusion PDE (4) becomes the eigenproblem

$$-v_{xx} + \lambda v = 0, \quad \text{such that } [v] = [v_x] + 2v = 0 \text{ at } x = 0, \quad (10)$$

with homogeneous Dirichlet boundary conditions $v(\pm 1) = 0$.

- Corresponding to eigenvalue $\lambda = 0$ is the neutral solution $v \propto 1 - |x|$ corresponding to a basis of the subspace \mathbb{E} of equilibria.
- Some negative eigenvalues $\lambda = -k^2$ correspond to eigenfunctions of the form $v \propto \sin[k(1 - |x|)]$. These arise by necessity from the PDE, the homogeneous Dirichlet boundary conditions, and the continuity of v . By straightforward algebra, the jump in the derivative determines the wavenumbers k from the solutions of $k = \tan k$, namely the wavenumbers $k = 4.4934, 7.7253, 10.9041, \dots$. That is, non-zero eigenvalues of the linearised problem are $\lambda = -20.191, -59.680, -118.900, \dots$. Fig. 2 plots (solid) the two eigenfunctions corresponding to the two of these eigenvalues of smallest magnitudes.
- Negative eigenvalues also arise from eigenfunctions of the form $v \propto \sin(kx)$. The boundary and coupling conditions determine the wavenumbers $k = n\pi$ for $n = 1, 2, 3, \dots$. That is, the other non-zero eigenvalues are $\lambda = -\pi^2, -4\pi^2, -9\pi^2, \dots$. Fig. 2 plots (dashed) the two eigenfunctions corresponding to the two of these eigenvalues of smallest magnitude.

One of the beautiful properties of the coupling conditions (8) is that with them the diffusion operator $\partial^2/\partial x^2$ is self-adjoint (Lemma 2, p. 7). Hence there are only real eigenvalues of the linear problem (10), namely the ones found above. To confirm self-adjointness under the usual inner product, $\langle u, v \rangle = \int_{-1}^1 u(x)v(x)dx$, consider

$$\begin{aligned} \langle u, v_{xx} \rangle &= \int_{-1}^1 uv_{xx} dx \quad (\text{then using integration by parts}) \\ &= [uv_x - vu_x]_{-1}^{0-} + [uv_x - vu_x]_{0+}^1 + \int_{-1}^1 u_{xx}v dx \\ &\quad (\text{using the Dirichlet boundary conditions}) \\ &= -[uv_x - vu_x]_{0-}^{0+} + \langle u_{xx}, v \rangle \\ &\quad (\text{using continuity at } x = 0) \\ &= -u|_0[v_x] + v|_0[u_x] + \langle u_{xx}, v \rangle \\ &\quad (\text{using the jump in derivative at } x = 0) \\ &= u|_0 2(1 - \gamma)v|_0 - v|_0 2(1 - \gamma)u|_0 + \langle u_{xx}, v \rangle \\ &= \langle u_{xx}, v \rangle. \end{aligned}$$

This useful self-adjointness is a property of previous holistic discretisations (e.g. [24], Part V), with the exception of the unusual coupling proposed by [23]. Preserving self-adjointness is a new feature established by the new approach developed herein.

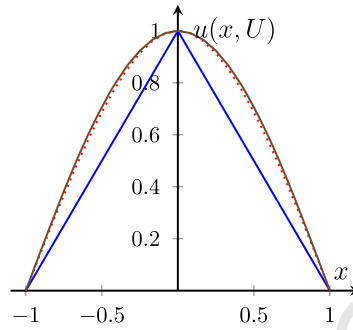


Fig. 3. A comparison of approximations to the long-term, quasi-stationary, decay of the heat PDE: blue-solid, $u \propto 1 - |x|$ is the basic linear approximation (9); red-dotted, the derived cubic spline (11) at full coupling $\gamma = 1$; and, almost indistinguishable, brown-solid, is the exact mode $u \propto \cos(\pi x/2)$.

Because the spectrum consists of a zero eigenvalue and all the rest negative ($-\pi^2 < -9$), the manifold theory (e.g. [5,11]) assures us that there exists a slow manifold in some neighbourhood of the subspace \mathbb{E} of equilibria (corresponding to Theorem 6); that is, global in amplitude U and local in parameters γ and α . Also, the theory guarantees that all solutions in the neighbourhood are attracted exponentially quickly, at least as fast as roughly $e^{-\pi^2 t}$, to solutions on the slow manifold. That is, the slow manifold and the evolution thereon emerges from general initial conditions.

A theorem (e.g. [5], Thm. 6.10) also guarantees that when we approximate the slow manifold and its evolution to a residual of $\mathcal{O}(\gamma^p)$, the slow manifold and its evolution are correct to errors $\mathcal{O}(\gamma^p)$. By straightforward machinations not detailed here ([20,24], Ch. 14) we arrive at the expressions that the slow manifold and the evolution thereon are

$$u \approx \left[1 - |x| + \gamma(|x| - \frac{3}{2}x^2 + \frac{1}{2}|x|^3) \right] U \quad \text{such that } \dot{U} \approx -3\gamma U. \quad (11)$$

Substituting these expressions into the heat PDE (4) ($\alpha = 0$), with the boundary and coupling conditions (8) we find the equations are satisfied to residual $\mathcal{O}(\gamma^2)$ and so the approximation theorem asserts these expressions are approximations with errors $\mathcal{O}(\gamma^2)$.

Although this approximation is based around parameter $\gamma = 0$, we are interested in the physical value of the parameter $\gamma = 1$. Evaluating the slow manifold (11) at $\gamma = 1$ gives

$$u \approx (1 - \frac{3}{2}x^2 + \frac{1}{2}|x|^3)U \quad \text{such that } \dot{U} \approx -3U.$$

The field u , plotted in Fig. 3, is an excellent cubic spline approximation to the correct $U \cos(\pi x/2)$ eigenfunction, also plotted in Fig. 3. The predicted evolution $U \propto e^{-3t}$ is a good approximation to the correct decay rate of $-\pi^2/4$.

One key question is how can we be sure that evaluating at finite $\gamma = 1$ is within the finite neighbourhood of validity of the slow manifold? Here computer algebra ([20,24], Ch. 14) straightforwardly computes to high order to determine, for example, the slow evolution

$$\dot{U} = -[3\gamma - 0.6\gamma^2 + 0.06857\gamma^3 - 0.00128\gamma^5 + 0.00008\gamma^6 + 0.00004\gamma^7 + \mathcal{O}(\gamma^8)]U.$$

Evidently the series in γ appears to have a radius of convergence much larger than one. Construction of the slow manifold to 40th order in γ (for $\alpha = 0$) followed by a generalised Domb-Sykes plot ([16], Appendix) predicts a convergence limiting singularity at $\gamma_* = -0.9 + i3.7$ (at an angle 103° to the real γ -axis) indicating convergence for all $|\gamma| < 3.8$. Hence we predict that the neighbourhood of validity around \mathbb{E} includes the case of interest, $\gamma = 1$.

Centre manifold theory (e.g. [5,24], Ch. 4) was designed for nonlinear problems. Thus it also applies here to the nonlinear Burgers' PDE (4) now with nonlinearity parametrised by α and similarly modelled with two intervals on the domain $-1 < x < 1$. For example, modified computer algebra ([20,24], Ch. 14) constructs the slow manifold plotted in Fig. 4 on which the nonlinear evolution is

$$\dot{U} = -(3\gamma - \frac{3}{5}\gamma^2)U - \frac{1}{15}\gamma^2\alpha^2U^3 + \mathcal{O}(\gamma^3 + \alpha^3) \quad (12)$$

The nonlinear advection of Burgers' PDE generates steeper gradients in the subgrid field (Fig. 4) that enhance the decay. Such enhanced decay is expressed by the cubic nonlinearity in the evolution equation (12) for amplitude $U(t)$ (cf. [12], §5).

One important generic feature of the evolution (12) is that the enhanced decay has coefficient α^2 —it is nonlinear in the coefficient α of the original Burgers' PDE (4). In general, an exact, closed, coarse scale, low-dimensional model is a nonlinear transformation of the detailed microscale equations, even when the dynamics are linear (e.g. [22]). Consequently, all dimensional reduction methods that rely on linear projection onto subspaces are generally and necessarily limited in accuracy—a limitation avoided by the nonlinear modelling methodology developed herein.

Key properties of this example are also exhibited in the application of the approach to the more general spatial discretisations discussed in subsequent sections: an analogous inter-element coupling engenders an emergent slow manifold; the

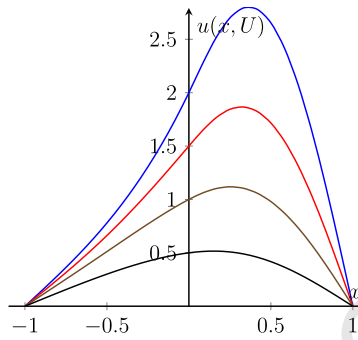


Fig. 4. Nonlinear slow manifold for Burgers' PDE (4) for viscosity $\nu = 1$ and nonlinearity $\alpha = 2$. Drawn is the slow manifold $u(x, U)$ for representative amplitudes $U = \frac{1}{2}, 1, \frac{3}{2}, 2$ to show the larger deformation at larger amplitudes. This approximation to the slow manifold was computed to errors $\mathcal{O}(\gamma^3 + \alpha^3)$ and evaluated at full coupling $\gamma = 1$.

linearised operator is self-adjoint; the first iteration constructs a cubic spline; and the resultant model at full coupling has attractive properties.

3. Linearisation establishes the existence of a closure

We use centre manifold theory (e.g. [5,11]) to newly establish (Theorem 6) the in-principle existence and emergence of an exact closure to the dynamics of PDEs in the class (1). Centre manifold theory is based upon an equilibrium or subspace of equilibria, and follows primarily from the local persistence of a spectral gap from that of the linearised dynamics (e.g. [24]).

To find useful equilibria we embed the PDE (1) in a wider class of problems. First partition the spatial domain into N intervals between the grid-points $x = X_j$, possibly unevenly spaced: let the interval $\mathbb{X}_j := \{x \mid X_{j-1} < x < X_j\}$ be of length $H_j := X_j - X_{j-1}$ and denote the punctured domain $\tilde{\mathbb{X}} := \mathbb{X} \setminus \{X_0, X_1, \dots, X_N\}$. For definiteness of theory take the boundary conditions to be that the field $u(x, t)$ is L -periodic in space. Then use $u_j(x, t)$ to denote solutions of the PDE (1) on the interval \mathbb{X}_j , and reserve $u(x, t)$, over \mathbb{X} or $\tilde{\mathbb{X}}$ as appropriate, to denote the union over all intervals of such solutions. To restore the original PDE (1) over the whole domain \mathbb{X} we couple the fields on each interval together. By controlling the information flow between intervals we connect the original PDE over the whole domain to a useful base problem. The general coupling conditions are of continuity and a crafted jump in derivative:

$$u(X_j^-, t) = u(X_j^+, t), \quad \text{and} \quad (13a)$$

$$\frac{(vu_x)|_{X_j^+}}{H_{j+1}} - \frac{(vu_x)|_{X_j^-}}{H_j} = C(\gamma) \left[\frac{(vu)|_{X_{j+1}^-} - (vu)|_{X_j^+}}{H_{j+1}^2} + \frac{(vu)|_{X_{j-1}^+} - (vu)|_{X_j^-}}{H_j^2} \right], \quad (13b)$$

where coefficient $\nu(x) = F'(u_x)$ is the effective diffusivity at each $x \in \tilde{\mathbb{X}}$, via the gradient u_x , and where the factor $C(\gamma)$ is some smooth function such that $C(0) = 1$ and $C(1) = 0$ (typically $C(\gamma) := 1 - \gamma$ as in (8)).

Lemma 1 (Equilibria). The PDE (1) on domain $\tilde{\mathbb{X}}$ with coupling conditions (13) possesses an N -dimensional subspace \mathbb{E} of equilibria, parametrised by $\tilde{U} = (U_1, U_2, \dots, U_N)$, for parameters $\alpha = \gamma = 0$. Each equilibrium is of continuous, piecewise linear, fields $u^*(x)$ such that, on the j th interval, the field

$$u^*(x) = u_j^*(x) = (1 - \xi_j)U_{j-1} + \xi_j U_j \quad \text{where } \xi_j = (x - X_{j-1})/H_j \quad (14)$$

is a local scaled space variable ($0 \leq \xi_j \leq 1$ for $x \in \mathbb{X}_j$).

Proof. With nonlinearity $\alpha = 0$ the PDE (1) takes the form $u_t = F(u_x)_x$. For the piecewise linear field (14), the gradient $u_{jx}^* = (U_j - U_{j-1})/H_j$ is constant on each \mathbb{X}_j . Hence $F(u_x^*)$ is constant on each \mathbb{X}_j , and consequently $F(u_x^*)_x = 0$ on $\tilde{\mathbb{X}}$, giving an equilibria of the PDE on $\tilde{\mathbb{X}}$.

From the field (14), for all j , $u_j^*(X_j^-) = U_j = u_{j+1}^*(X_j^+)$ and hence $u^*(x)$ is continuous at X_j to satisfy the coupling condition (13a).

Lastly, consider the condition (13b) on the jump in the derivative for all j . For the field (14), the gradient is $u_x^* = (U_j - U_{j-1})/H_j$ so, in terms of the effective diffusivity constants

$$\nu_j := F'(u_{jx}^*) = F'\left(\frac{U_j - U_{j-1}}{H_j}\right), \quad (15)$$

the jump in gradient

$$\begin{aligned}
 & \frac{(vu_x^*)|_{X_j^+}}{H_{j+1}} - \frac{(vu_x^*)|_{X_j^-}}{H_j} \\
 &= \frac{v_{j+1}}{H_{j+1}} \frac{U_{j+1} - U_j}{H_{j+1}} - \frac{v_j}{H_j} \frac{U_j - U_{j-1}}{H_j} \\
 &= \frac{v_{j+1}U_{j+1} - v_{j+1}U_j}{H_{j+1}^2} + \frac{v_jU_{j-1} - v_jU_j}{H_j^2} \\
 &= \frac{1}{H_{j+1}^2} \left[(vu^*)|_{X_{j+1}^-} - (vu^*)|_{X_j^+} \right] + \frac{1}{H_j^2} \left[(vu^*)|_{X_{j-1}^+} - (vu^*)|_{X_j^-} \right],
 \end{aligned}$$

which is the required right-hand side of (13b) at coupling parameter $\gamma = 0$ (since $C(0) = 1$). Hence, the piecewise linear fields (14), with $\alpha = \gamma = 0$, are equilibria for all \bar{U} , and thus form an N -D subspace of equilibria. \square

The spectrum comes from the linearised dynamics around each of the equilibria \mathbb{E} . Seek solutions $u = u^*(x) + \hat{u}(x, t)$ of the general PDE (1) where $\hat{u}(x, t)$ denotes a small perturbation to the equilibrium (14). Use $\hat{u}_j(x, t)$ as a synonym for $\hat{u}(x, t)$ on the j th interval \mathbb{X}_j . Then for parameters $\alpha = \gamma = 0$ and small \hat{u} , the PDE (1) linearises to

$$\hat{u}_t = F'(u_x^*)\hat{u}_{xx} = v(x)\hat{u}_{xx} \quad \text{on } \tilde{\mathbb{X}}; \quad \text{that is, } \hat{u}_{jt} = v_j\hat{u}_{jxx} \text{ for } x \in \mathbb{X}_j. \quad (16a)$$

The coupling conditions (13) are linear, so for the perturbations they are (with time t implicit for brevity)

$$\hat{u}_{j+1}(X_j) = \hat{u}_j(X_j), \quad \text{and} \quad (16b)$$

$$\frac{v_{j+1}\hat{u}_{j+1,x}(X_j)}{H_{j+1}} - \frac{v_j\hat{u}_{j,x}(X_j)}{H_j} = \frac{v_{j+1}\hat{u}_{j+1}(X_{j+1}) - v_{j+1}\hat{u}_{j+1}(X_j)}{H_{j+1}^2} + \frac{v_j\hat{u}_j(X_{j-1}) - v_j\hat{u}_j(X_j)}{H_j^2}. \quad (16c)$$

The next lemma certifies that this linearised system (16) is self-adjoint and so we need only seek real eigenvalues in the spectrum.

To be definite, define the Hilbert space \mathbb{H} to be the set of square integrable, twice differentiable, functions on $\tilde{\mathbb{X}}$. Also define its subspace \mathbb{L} to be those which are additionally L -periodic.

Lemma 2 (Self-adjoint). *The differential operator appearing in (16), namely $\mathcal{L} = v\partial^2/\partial x^2$ on \mathbb{L} and subject to (16b)–(16c), is self-adjoint in the interval-weighted inner product $\langle v, u \rangle := \sum_j \frac{1}{H_j} \int_{\mathbb{X}_j} vu \, dx$.*

Proof. Straightforwardly use integration by parts (remembering that v is piecewise constant in (16)):

$$\begin{aligned}
 \langle v, \mathcal{L}u \rangle &= \sum_j \frac{1}{H_j} \int_{\mathbb{X}_j} v v u_{xx} \, dx \\
 &= \sum_j \frac{1}{H_j} [v v u_x - v u v_x]_{X_{j-1}^+}^{X_j^-} + \sum_j \frac{1}{H_j} \int_{\mathbb{X}_j} v v_{xx} u \, dx \\
 &= \sum_j \frac{1}{H_j} [v_j v_j (X_j^-) u_{jx}(X_j^-) - v_j u_j (X_j^-) v_{jx}(X_j^-) \\
 &\quad - v_j v_j (X_{j-1}^+) u_{jx}(X_{j-1}^+) + v_j u_j (X_{j-1}^+) v_{jx}(X_{j-1}^+)] + \langle \mathcal{L}v, u \rangle \\
 &\quad \text{(use the continuity (16b) and } U_j := u(X_j^\pm), \, V_j := v(X_j^\pm)) \\
 &= \sum_j \frac{1}{H_j} [v_j V_j u_{jx}(X_j^-) - v_j U_j v_{jx}(X_j^-) - v_j V_{j-1} u_{jx}(X_{j-1}^+) + v_j U_{j-1} v_{jx}(X_{j-1}^+)] + \langle \mathcal{L}v, u \rangle \\
 &\quad \text{(reindex the last two terms in the sum, } j \mapsto j+1) \\
 &= \sum_j \left[\frac{V_j v_j u_{jx}(X_j^-)}{H_j} - \frac{U_j v_j v_{jx}(X_j^-)}{H_j} - \frac{V_j v_{j+1} u_{j+1,x}(X_j^+)}{H_j} + \frac{U_j v_{j+1} v_{j+1,x}(X_j^+)}{H_j} \right] + \langle \mathcal{L}v, u \rangle \\
 &\quad \text{(replace two pairs of terms via coupling (16c))}
 \end{aligned}$$

$$\begin{aligned}
&= \sum_j \left\{ -V_j \left[\frac{v_{j+1}U_{j+1} - v_{j+1}U_j}{H_{j+1}^2} + \frac{v_jU_{j-1} - v_jU_j}{H_{j+1}^2} \right] \right. \\
&\quad \left. + U_j \left[\frac{v_{j+1}V_{j+1} - v_{j+1}V_j}{H_j^2} + \frac{v_jV_{j-1} - v_jV_j}{H_j^2} \right] \right\} + \langle \mathcal{L}v, u \rangle \\
&\quad \text{(cancel four terms in } U_jV_j) \\
&= \sum_j \left\{ -\frac{V_jv_{j+1}U_{j+1}}{H_{j+1}^2} - \frac{V_jv_jU_{j-1}}{H_j^2} + \frac{U_jv_{j+1}V_{j+1}}{H_{j+1}^2} + \frac{U_jv_jV_{j-1}}{H_j^2} \right\} + \langle \mathcal{L}v, u \rangle \\
&\quad \text{(reindex 2nd and 4th terms, } j \mapsto j+1, \text{ and cancel)} \\
&= \sum_j 0 + \langle \mathcal{L}v, u \rangle = \langle \mathcal{L}v, u \rangle.
\end{aligned}$$

Hence, the linear operator in the linearised system (16) is self-adjoint. Since $\mathcal{L}: \mathbb{H} \rightarrow \mathbb{H}$ it is self-adjoint in \mathbb{H} . \square

It can be shown that self-adjointness also holds for Dirichlet and Neumann boundary conditions.

We turn to determining the spectrum of the general linearised system (16): first, the zero eigenvalues; and second, the non-zero eigenvalues. Because of the N -D subspace of equilibria \mathbb{E} , the linearised system must have N eigenvalues of zero. Corresponding basis eigenfunctions may be chosen to be the ‘triangular’

$$\phi_j(x) = \max \{0, 1 - \max [(X_j - x)/H_j, (x - X_j)/H_{j+1}]\}$$

so the equilibria (14) may be written $u^* = \sum_j \phi_j(x)U_j$. Incidentally, the localised triangular shape of these basis functions will be recognised by many as the fundamental “shape function” often invoked in the finite element method (e.g. [17,28]). For the linearised PDE (16a) any eigenfunction corresponding to an eigenvalue of zero must be linear on each \mathbb{X}_j , and the continuity (16b) then guarantees there are no other eigenfunctions than those identified. By self-adjointness, there are no generalised eigenfunctions. Thus the slow subspace of the system (16) is N -D, namely \mathbb{E} .

For rigorous theory we notionally adjoin the two trivial dynamical equations $\alpha_t = \gamma_t = 0$ to the linearised system (16). Then, as $\alpha = \gamma = 0$, the equilibria (14) are $(0, 0, u^*(x))$. Thus strictly there are two extra zero eigenvalues associated with the trivial $\alpha_t = \gamma_t = 0$, and the corresponding slow subspace of each equilibria is $(N+2)$ -D. Except for issues associated with the domain of validity, for simplicity we do not explicitly include these two trivial dynamical equations nor their eigenvalues in the following, but consider them implicit.

Lemma 3 (exponential dichotomy). *Provided function F in the PDE (1) is monotonically increasing, then the operator $\mathcal{L} = v\partial^2/\partial x^2$ subject to (16b)–(16c) in \mathbb{L} has N zero eigenvalues and all other eigenvalues λ are negative and bounded away from zero by $\lambda \leq -\beta$ where bound $\beta := \min_j (\pi^2 v_j / H_j^2) > 0$.*

Proof. The precisely N zero eigenvalues are established in the two paragraphs preceding the lemma. Lemma 2 establishes all eigenvalues of \mathcal{L} are real. Let λ be a non-zero eigenvalue and $v(x)$ be a corresponding eigenfunction. Then $v \perp \mathbb{E}$ by self-adjointness of \mathcal{L} , and, as usual,

$$(-\lambda)\|v\|^2 = -\lambda \langle v, v \rangle = \langle v, -\lambda v \rangle = \langle v, -\mathcal{L}v \rangle.$$

Decompose the eigenfunction into $v(x) = \tilde{v}(x) + \check{v}(x)$ where $\check{v}(x) \in \mathbb{E}$, that is piecewise linear and continuous, and further satisfies $\check{v}(X_j) = v(X_j)$. Consequently, the other component \tilde{v} is also continuous, and further satisfies $\tilde{v}(X_j) = 0$. Since $\check{v} \in \mathbb{E}$, so $\mathcal{L}\check{v} = 0$ (the check accent on \check{v} is to remind us of its piecewise linear nature). Consequently,

$$\begin{aligned}
-\lambda\|v\|^2 &= \langle v, -\mathcal{L}v \rangle = \langle \tilde{v} + \check{v}, -\mathcal{L}\tilde{v} \rangle \\
&= \langle \tilde{v}, -\mathcal{L}\tilde{v} \rangle + \langle \check{v}, -\mathcal{L}\tilde{v} \rangle \\
&= \langle \tilde{v}, -\mathcal{L}\tilde{v} \rangle
\end{aligned}$$

as, by self-adjointness, $\langle \check{v}, -\mathcal{L}\tilde{v} \rangle = \langle \mathcal{L}\check{v}, -\tilde{v} \rangle = \langle 0, -\tilde{v} \rangle = 0$. Thus, we proceed to derive the inequality

$$-\lambda\|v\|^2 = \langle \tilde{v}, -\mathcal{L}\tilde{v} \rangle = \sum_j \frac{1}{H_j} \int_{\mathbb{X}_j} -v\tilde{v}_{xx} dx$$

$$\begin{aligned}
&= \sum_j [-v \tilde{v}_x]_{X_{j-1}^+}^{X_j^-} + \sum_j \frac{1}{H_j} \int_{\mathbb{X}_j} v \tilde{v}_x^2 dx \quad (\text{integrating by parts}) \\
&= \sum_j 0 + \sum_j \frac{1}{H_j} \int_{\mathbb{X}_j} v \tilde{v}_x^2 dx \quad (\text{using } \tilde{v}(X_j^-) = \tilde{v}(X_j^+) = 0) \\
&= \sum_j \frac{v_j}{H_j^2} \frac{1}{H_j} \int_{\mathbb{X}_j} H_j^2 \tilde{v}_x^2 dx \quad (\text{as } v(x) \text{ is piecewise constant}) \\
&\geq \frac{\beta}{\pi^2} \sum_j \frac{1}{H_j} \int_{\mathbb{X}_j} H_j^2 \tilde{v}_x^2 dx, \tag{17a}
\end{aligned}$$

for bound β defined by Lemma 3. The first consequence of this inequality is that there are no positive eigenvalues λ .

Secondly, relate this inequality to the spatially homogeneous problem. Let \mathcal{L}_* denote the linear operator with coupling conditions appearing in (16) for the special case of $v(x) = H_j^2$ for all $x \in \mathbb{X}_j$; that is, $\mathcal{L}_* = H_j^2 \partial^2 / \partial x^2$ for $x \in \mathbb{X}_j$. Then, by the reverse argument to that of the previous paragraph,

$$\sum_j \frac{1}{H_j} \int_{\mathbb{X}_j} H_j^2 \tilde{v}_x^2 dx = \dots = \langle \tilde{v}, -\mathcal{L}_* \tilde{v} \rangle = \dots = \langle v, -\mathcal{L}_* v \rangle. \tag{17b}$$

But, by the Rayleigh–Ritz theorem, the smallest magnitude, non-zero, eigenvalue λ_1 of \mathcal{L}_* satisfies $-\lambda_1 = \min_{w \perp \mathbb{E}} \langle w, -\mathcal{L}_* w \rangle / \|w\|^2$, and so

$$\langle v, -\mathcal{L}_* v \rangle \geq -\lambda_1 \|v\|^2. \tag{17c}$$

Hence the inequalities (17a)–(17c) give $-\lambda \|v\|^2 \geq \frac{\beta}{\pi^2} (-\lambda_1) \|v\|^2$. By the next Lemma 4, $-\lambda_1 \geq \pi^2$, and so all non-zero eigenvalues satisfy $-\lambda \geq \beta$ as required. That the bound $\beta > 0$ follows from (15) and the monotonicity of F : $v_j = F'(u_{jx}^*) > 0$ for all j , and so $\min_j (v_j / H_j^2) > 0$. \square

Lemma 4 (reference spectrum). Consider the differential operator \mathcal{L}_* with coupling conditions (16b)–(16c) in \mathbb{H} , for which $v_j \mapsto H_j^2$: the non-zero eigenvalues of \mathcal{L}_* all satisfy $\lambda \leq -\pi^2$.

Proof. Seeking solutions $\hat{u} = e^{\lambda t} v(x)$ leads to the ODEs $\lambda v_j = H_j^2 v_j''$ on \mathbb{X}_j . As a piecewise constant coefficient ODE, and setting eigenvalues $\lambda = -\kappa^2$ for some $\kappa \geq 0$ to be determined, its general solutions are of the form $v_j = A_j \cos \kappa \xi_j + B_j \sin \kappa \xi_j$ for coefficients A_j and B_j determined by the coupling conditions (16b)–(16c). Consequently, the spatial derivative is $v_{jx} = -\frac{A_j \kappa}{H_j} \sin \kappa \xi_j + \frac{B_j \kappa}{H_j} \cos \kappa \xi_j$. Let's consider the spatial map $(A_j, B_j) \mapsto (A_{j+1}, B_{j+1})$. Continuity (16b) at $x = X_j$ ($\xi_j = 1$) requires

$$A_{j+1} = A_j \cos \kappa + B_j \sin \kappa = c A_j + s B_j, \tag{18a}$$

where, for brevity in this proof, let $c := \cos \kappa$ and $s := \sin \kappa$. The derivative jump (16c) at $x = X_j$, with $v_j = H_j^2$, requires

$$\begin{aligned}
&H_{j+1}^2 \frac{\kappa B_{j+1} / H_{j+1}}{H_{j+1}} - H_j^2 \frac{-(\kappa A_j / H_j) s + (\kappa B_j / H_j) c}{H_j} \\
&= C(\gamma) \left\{ \frac{1}{H_{j+1}^2} [H_{j+1}^2 (c A_{j+1} + s B_{j+1}) - H_{j+1}^2 A_{j+1}] + \frac{1}{H_j^2} [H_j^2 A_j - H_j^2 (c A_j + s B_j)] \right\},
\end{aligned}$$

where we include the factor $C(\gamma)$ for a little more generality. This requirement rearranges to

$$\kappa B_{j+1} + \kappa s A_j - \kappa c B_j = C(\gamma) [c A_{j+1} + s B_{j+1} - 2 A_{j+1} + A_j],$$

$$\text{that is, } (c - 2) C A_{j+1} + (Cs - \kappa) B_{j+1} + (C - s\kappa) A_j + c\kappa B_j = 0.$$

Dividing by C and setting $\kappa' = \kappa / C$ gives the equivalent

$$(c - 2) A_{j+1} + (s - \kappa') B_{j+1} + (1 - s\kappa') A_j + c\kappa' B_j = 0. \tag{18b}$$

Consider together the two mapping equations (18a)–(18b): this spatial map has solutions $(A_j, B_j) \propto \mu^j$ for some multipliers μ given by the vanishing of the determinant

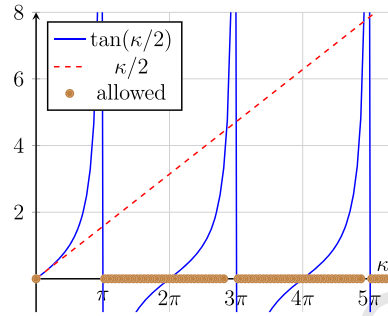


Fig. 5. The linearised ($\gamma = 0$, $C = 1$) spectrum determined by the spectral requirement (18d). The thick lines along the κ -axis indicate regions of spatial wavenumbers for which the corresponding spatial structures are bounded for all space (the essential spectrum).

$$\det \begin{bmatrix} \mu - c & -s \\ \mu(c-2) + 1 - s\kappa' & \mu(s - \kappa') + c\kappa' \end{bmatrix} = 0;$$

$$\text{that is, } \mu^2 - 2\frac{s - c\kappa'}{s - \kappa'}\mu + 1 = 0. \quad (18c)$$

Hence the two possible multipliers of the spatial map are

$$\mu = \rho \pm \sqrt{\rho^2 - 1} \quad \text{for ratio } \rho = \frac{s - c\kappa'}{s - \kappa'}.$$

Now $|\rho| > 1$ is not possible as then there would be two (real) multipliers: one with magnitude greater than one, representing structures growing exponentially quickly to the right; and one with magnitude less than one, representing structures growing exponentially quickly to the left. The only allowable cases occur for $|\rho| \leq 1$ when the multipliers are complex of unit magnitude $|\mu| = 1$, and so characterise periodic structures in space. Since $\kappa' - s = \kappa/C(\gamma) - \sin \kappa \geq 0$, the requirement $|\rho| \leq 1$ becomes $s - \kappa' \leq c\kappa' - s \leq \kappa' - s$; that is, $2s - \kappa' \leq c\kappa' \leq \kappa'$. The right-hand inequality is always satisfied as $c = \cos \kappa$. The left-hand inequality requires $2s \leq (1 + c)\kappa'$, that is, $s/(1 + c) \leq \kappa'/2$. Recalling $s = \sin \kappa$ and $c = \cos \kappa$, this requirement becomes

$$\tan \frac{\kappa}{2} \leq \frac{\kappa}{2C}. \quad (18d)$$

The specific boundary conditions on the finite macroscale domain \mathbb{X} then constrain the allowable κ to a discrete, countably infinite, set of κ satisfying inequality (18d). As illustrated by Fig. 5, for the specific case of the linearised problem (16) for which $C(0) = 1$, there is a useful spectral gap because the smallest allowable nonzero nondimensional wavenumber is $\kappa = \pi$. Hence the smallest magnitude nonzero eigenvalue is $\leq -\pi^2$ as required. \square

The reason to include $C(\gamma)$ in the proof is to comment on the linearisation about another subspace of equilibria. As well as the piecewise linear equilibria \mathbb{E} at $\gamma = \alpha = 0$, another subspace of equilibria is $u = \text{constant}$ on \mathbb{X} for nonlinearity $\alpha = 0$ but now for arbitrary coupling parameter γ . The linearisation about this set of equilibria is also the system (16) but with $v(x) = F'(0)$, constant, and with the right-hand side of the coupling (16c) multiplied by $C(\gamma)$. The proof of Lemma 4 also applies to this case. Inequality (18d) then gives allowed wavenumbers for general γ . As coupling parameter γ varies from zero to one, the factor $C(\gamma)$ varies from one to zero, and so the denominator C in inequality (18d) increases the slope of the straight line of Fig. 5. Thus the set of allowed wavenumbers increases with coupling γ , and, in particular, the spectral gap $(0, \pi)$ between the slow and the fast modes fills up with the slow modes. It is in this manner that the continuum of allowed wavenumbers is restored in the fully coupled PDE over the whole domain \mathbb{X} , as the coupling parameter γ varies from zero to one.

Hypothesis 5. The following Theorem 6 relies upon theorems by [11] which in turn require certain preconditions listed here that need to hold. We consider twice differentiable, L -periodic, square integrable functions on \mathbb{X} which forms the requisite Hilbert spaces ($\mathcal{Z} \hookrightarrow \mathcal{Y} \hookrightarrow \mathcal{X} = \mathbb{L}$). Then the self-adjoint, linearised operator (16) of diffusion on a finite spatial domain forms an analytic semigroup (e.g. [11], Remark

1. Spectral Decomposition Hypothesis 2.4 of [11], consider the spectrum σ of the linear operator and assume that
 - (a) there exists a constant $\beta > 0$ such that

$$\inf_{\{\lambda \in \sigma : \Re \lambda > 0\}} \Re \lambda > \beta, \quad \text{and} \quad \sup_{\{\lambda \in \sigma : \Re \lambda < 0\}} \Re \lambda < -\beta;$$

- (b) the set $\{\lambda \in \sigma : \Re \lambda = 0\}$ consists of a finite number of eigenvalues with finite algebraic multiplicity.
2. Hypothesis 2.1 of [11]: (i) $\mathcal{L} \in \mathcal{L}(\mathcal{Z}, \mathcal{X})$; and (ii) writing a system as $du/dt = \mathcal{L}u + R(u)$, for some $q \geq 2$ there exists a neighbourhood $\mathcal{V} \subset \mathcal{Z}$ of the origin such that $R \in C^q(\mathcal{V}, \mathcal{Y})$ and that $R(0) = 0$ and $DR(0) = 0$.
3. In the case of non-autonomous nonlinearity (R becomes $R(u, t)$), Hypothesis 3.8(ii) of [11] additionally assumes that for any sufficiently small ε , there exist positive constants $\delta_0(\varepsilon) = \mathcal{O}(\varepsilon^2)$ and $\delta_1(\varepsilon) = \mathcal{O}(\varepsilon)$ such that

$$\sup_{u \in B_\varepsilon(\mathcal{Z})} \|R(u, t)\|_{\mathcal{Y}} = \delta_0(\varepsilon), \quad \sup_{u \in B_\varepsilon(\mathcal{Z})} \|D_u R(u, t)\|_{\mathcal{L}(\mathcal{Z}, \mathcal{Y})} = \delta_1(\varepsilon).$$

Theorem 6 (Slow manifold). Consider the nonlinear PDE (1) on domain $\tilde{\mathbb{X}}$ with coupling conditions (13) and assume that the functions F and G of the PDE (1) are smooth enough so that for every $u^* \in \mathbb{E}$ the nonlinear function $R(u, t) := F(u_x^* + u_x)_x - \mathcal{L}u + \alpha G(t, u^* + u)$ satisfies Hypothesis 5.2 and Hypothesis 5.3.

1. In an open domain \mathcal{E} containing the subspace \mathbb{E} there exists a slow manifold,

$$u = u(x, t, \tilde{U}, \gamma, \alpha) \quad \text{such that} \quad \frac{d\tilde{U}}{dt} = \tilde{g}(\tilde{U}, t, \gamma, \alpha) \quad (19)$$

(generally as smooth as F and G).

2. This slow manifold is emergent in the sense that for all solutions $u(x, t)$ of (1) and (13), that stay in \mathcal{E} , there exists a solution $\tilde{U}(t)$ of (19) such that $u(x, t) = u(x, t, \tilde{U}(t), \gamma, \alpha) + \mathcal{O}e^{-\beta' t}$ for decay rate $0 < \beta' < \beta$ (from Lemma 3).
3. Given two smooth functions $\tilde{u}(x, t, \tilde{U}, \gamma, \alpha)$ and $\tilde{g}(\tilde{U}, t, \gamma, \alpha)$ for the governing equations (1) and (13), evaluated at $u = \tilde{u}$ such that $d\tilde{U}/dt = \tilde{g}$, having residuals $\mathcal{O}\gamma^p + \alpha^q$ as $(\gamma, \alpha) \rightarrow \vec{0}$, then the slow manifold is

$$u = \tilde{u}(x, \tilde{U}, \gamma, \alpha) + \mathcal{O}\gamma^p + \alpha^q \quad \text{s.t.} \quad \frac{d\tilde{U}}{dt} = \tilde{g}(\tilde{U}, t, \gamma, \alpha) + \mathcal{O}\gamma^p + \alpha^q.$$

Proof. Lemma 3 establishes the Spectral Decomposition Hypothesis 5.1 (from [11]) for all $u^* \in \mathbb{E}$.

1. Theorem 2.9 of [11] (Theorem 3.9 in the non-autonomous case) then establishes that for each point of \mathbb{E} (parametrised by \tilde{U}) a local centre manifold $\mathcal{M}_{\tilde{U}}$ exists in some neighbourhood $\mathcal{E}_{\tilde{U}}$ in the $(\tilde{U}, \gamma, \alpha)$ -space. Because the centre eigenvalues are all zero (Lemma 3), they are more precisely called *local slow manifolds*. Setting $\mathcal{M} := \bigcup_{\tilde{U}} \mathcal{M}_{\tilde{U}}$ and domain $\mathcal{E} := \bigcup_{\tilde{U}} \mathcal{E}_{\tilde{U}}$ the slow manifold \mathcal{M} exists in the domain \mathcal{E} (containing \mathbb{E}) as required.
2. The unstable spectrum is empty (Lemma 3), so Theorem 3.22 of [11] applies to establish the exponentially quick emergence of the slow manifold to all solutions that remain within \mathcal{E} for all time. By continuity in perturbations, the rate of attraction to the slow manifold in \mathcal{E} is estimated by the linearised rate β at \mathbb{E} [24, §11.3, e.g.].
3. Under corresponding preconditions, Proposition 3.6 of [18] proves that if an approximation to the slow manifold (19) gives residuals of the system's equations which are zero to some order, then the slow manifold is approximated to the same order of error. Here introduce parameter ϵ and set $\gamma = c\epsilon^q$ and $\alpha = a\epsilon^p$ for some chosen coefficients c and a , and some chosen exponents p and q . Then regard quantities as a Taylor series in ϵ with coefficients parametrised by (\tilde{U}, c, a) . Also, the process $\epsilon \rightarrow 0$ implies $(\gamma, \alpha) \rightarrow \vec{0}$. By supposition, the given \tilde{u} and \tilde{g} have residuals $\mathcal{O}\gamma^p + \alpha^q = \mathcal{O}c^p \epsilon^{pq} + a^q \epsilon^{pq} = \mathcal{O}\epsilon^{pq}$ as $\epsilon \rightarrow 0$. By Proposition 3.6 of [18], \tilde{u} and \tilde{g} approximate the slow manifold to errors $\mathcal{O}\epsilon^{pq}$, and hence the errors are $\mathcal{O}\gamma^p + \alpha^q$.

The more wide ranging theorems of [1–3] also be invoked to establish this theorem. \square

The evolution equation (19), evaluated at full coupling $\gamma = 1$, namely $d\tilde{U}/dt = g(\tilde{U}, t, 1, \alpha)$, is the in-principle exact closure for a discretisation of the dynamics of the nonlinear PDE (1).

3.1. The slow manifold of wave-like PDEs

Although this article's scope is the spatial discretisation, or dimensional reduction, of reaction–advection–diffusion PDEs (1), much of the theory usefully applies to the spatial discretisation of wave-like PDEs in the form

$$u_{tt} = F(u_x)_x + \alpha G(x, t, u, u_x) \quad (20)$$

on a domain \mathbb{X} , and for smooth functions F and G as before. This subsection comments on the similarities and differences of the theoretical support for such wave systems.

Partition space as above and apply the coupling conditions (13). Then, for $\alpha = \gamma = 0$, the subspace \mathbb{E} of piecewise linear equilibria of Lemma 1 still exists. Upon linearisation about each of these equilibria, the spatial differential operator $\mathcal{L} = v\partial^2/\partial x^2$ on $\tilde{\mathbb{X}}$ remains self-adjoint (Lemma 2). The exponential dichotomy of the operator \mathcal{L} (Lemmas 3 and 4) still

applies, namely that there are N eigenvalues of zero, and the others are $\leq -\beta$. So far, the considerations are the same for both diffusion systems and wave systems.

The differences in theoretical support start with Theorem 6. The reason for the differences are that the eigenvalues of the right-hand side operator \mathcal{L} are the square of the eigenvalues of the linearisation of the wave PDE (20): seeking waves of frequency ω then $|\omega| = \sqrt{-\lambda}$ and all frequencies ω are real as all eigenvalues are ≤ 0 . Here the slow manifold dichotomy is now between slow waves with near zero frequency, separated from fast waves with frequencies $\geq \sqrt{\beta}$. Such subcentre slow manifolds are ubiquitous in geophysical applications. However, much less is known rigorously about subcentre slow manifolds: even their existence is problematic [15]. Nonetheless, based upon recursively constructing coordinate transforms to a normal form ([6,7,24], Chap. 13) we make the following ‘backwards’ conjecture (e.g. [10,25]) for the wave PDE (20). Parts of this conjecture for waves correspond to Theorem 6 for dissipative systems.

Conjecture 7. Specify any order of error $\mathcal{O}(\gamma^p + \alpha^q)$. Then there exists a (multinomial) coordinate transformation and a (multinomial) PDE system in the new variables $(\tilde{U}, V(x))$ of the form

$$u = u(x, t, \tilde{U}, V, \gamma, \alpha), \quad \frac{d^2 \tilde{U}}{dt^2} = \tilde{g}(\tilde{U}, V, t, \gamma, \alpha), \quad \frac{\partial^2 V}{\partial t^2} = H(x, t, \tilde{U}, V, \gamma, \alpha)V, \quad (21)$$

such that in the u -space the corresponding dynamics is the same as the PDE (20) to an error $\mathcal{O}(\gamma^p + \alpha^q)$, and $u(x, t, \tilde{U}, 0, \gamma, \alpha)$ ($V = 0$) is tangent to the subspace \mathbb{E} at $\gamma = \alpha = 0$. (A difference with Theorem 6.3 is that here we posit a ‘nearby’ approximating system and then base results on that.)

1. Let \mathcal{E} denote a $u\gamma\alpha$ -domain in which the coordinate transform (21) is a diffeomorphism containing \mathbb{E} , then $V = 0$ is an exact slow manifold of the dynamics of (21): that is,

$$u = u(x, t, \tilde{U}, 0, \gamma, \alpha) \quad \text{such that} \quad \frac{d^2 \tilde{U}}{dt^2} = \tilde{g}(\tilde{U}, 0, t, \gamma, \alpha). \quad (22)$$

(A difference with Theorem 6.1 is that here there are nearby systems which have slow manifolds; although like the dissipative case, such a nearby system does possess an exact low-dimensional closure.)

2. Solutions near, but off the slow manifold with $V \neq 0$, generally evolve differently (due to wave-wave forcing of mean flow):

$$\frac{d^2 \tilde{U}}{dt^2} = \tilde{g}(\tilde{U}, 0, t, \gamma, \alpha) + \mathcal{O}(\|V\|^2).$$

(A difference with Theorem 6.2 is that here the slow manifold is not exponentially attractive and instead generally acts as a dynamical centre for nearby dynamics.)

Consequently, we contend that the methodology developed here for constructing and using spatially discrete, finite dimensional, models of dissipative PDEs may be also usefully applied to wave-like PDEs (20).

4. Example: nonlinear modelling of Burger's PDE

This section uses Burgers' PDE (4) as an example of the construction of a slow manifold discrete model. Burgers' PDE (4) is in the class (1) addressed by the theory of Section 3 and so Theorem 6 assures us a slow manifold model exists. Since Burgers' PDE is autonomous, here the slow manifold is independent of time—constructing non-autonomous slow manifolds is significantly more complicated (e.g. [4]). In this example we discretise on an equi-spaced grid with constant $H_j = H$.

4.1. Construct slow manifold discretisations

Proposition 3.6 by [18] underlies the construction as it asserts the order of error of an approximation is the same as the order of error of the residuals of the governing equations. Given the existence of a slow manifold $u = u(x, \tilde{U})$ such that $\tilde{U} = \tilde{g}(\tilde{U})$, and implicitly a function of coupling γ and nonlinearity α , we rewrite Burgers' PDE (4) in the form

$$\mathcal{R}(u, \tilde{g}) = 0 \quad \text{with residual } \mathcal{R}(u, \tilde{g}) := -\frac{\partial u}{\partial \tilde{U}} \cdot \tilde{g} + v \frac{\partial^2 u}{\partial x^2} - \alpha u u_x. \quad (23)$$

The initial approximation to the slow manifold is, in terms of the local space variable $\xi_j = (x - X_{j-1})/H$ defined by (14), the piecewise linear field

$$u^0 = \sum_{j=1}^N \chi_j(x) [(1 - \xi_j)U_{j-1} + \xi_j U_j] \quad \text{where } \chi_j(x) = \begin{cases} 1 & \text{if } x \in \mathbb{X}_j, \\ 0 & \text{if } x \notin \mathbb{X}_j. \end{cases} \quad (24)$$

We seek the slow manifold for the coupled and nonlinear dynamics in a multivariate power series corresponding parameters γ and α . But to simplify the algebraic construction process we follow the approach of [13] and introduce one ordering parameter $\varepsilon = \sqrt{\gamma^2 + \alpha^2}$ and label terms depending upon their order in ε . For example, a term in $\gamma^p \alpha^q$ is termed of order ε^{p+q} . Then we seek expressions for the slow manifold in the asymptotic series

$$u(x, \vec{U}, \gamma, \alpha) \sim \sum_{n=0}^{\infty} u^n(x, \vec{U}, \gamma, \alpha), \quad \vec{g}(\vec{U}, \gamma, \alpha) \sim \sum_{n=1}^{\infty} \vec{g}^n(\vec{U}, \gamma, \alpha), \quad (25)$$

where u^n and \vec{g}^n are of order n in the order parameter ε . The partial sums of these series are denoted by superscripts in parentheses:

$$u^{(n)}(x, \vec{U}, \gamma, \alpha) := \sum_{p=0}^n u^p, \quad \vec{g}^{(n)}(\vec{U}, \gamma, \alpha) := \sum_{p=1}^n \vec{g}^p. \quad (26)$$

Then $u = u^{(n)} + \mathcal{O}(\varepsilon^{n+1})$ and $u^{(n)} = u^{(n-1)} + u^n$; likewise for $\vec{g}^{(n)}$ and \vec{g}^n . Substituting these into the PDE-residual (23) and rearranging we deduce

$$\mathcal{R}(u^{(n)}, \vec{g}^{(n)}) = -\frac{\partial u^0}{\partial \vec{U}} \cdot \vec{g}^n + v \frac{\partial^2 u^n}{\partial x^2} + \mathcal{R}(u^{(n-1)}, \vec{g}^{(n-1)}) + \mathcal{O}(\varepsilon^{n+1}).$$

Hence to require the residual $\mathcal{R}(u^{(n)}, \vec{g}^{(n)}) = \mathcal{O}(\varepsilon^{n+1})$, the process is to iteratively solve

$$v \frac{\partial^2 u^n}{\partial x^2} = \frac{\partial u^0}{\partial \vec{U}} \cdot \vec{g}^n - \mathcal{R}(u^{(n-1)}, \vec{g}^{(n-1)}) \quad (27)$$

for corrections u^n to the subgrid field and corrections \vec{g}^n to the slow manifold closure of the evolution.

Computer algebra code listed in the Ancillary Material (Appendix A) confirms the following algebraic summary.

First order approximation Obtain the first approximation by solving (27) for the case $n = 1$ given the initial subspace approximation (24). Recalling the shift operator $\sigma U_j = U_{j+1}$ and defining the backward difference operator $\nabla := 1 - \sigma^{-1}$, equation (27) becomes

$$v \frac{\partial^2 u^1}{\partial x^2} = \sum_{j=1}^N \chi_j(x) \left\{ [\xi_j + (1 - \xi_j)\sigma^{-1}] g_j^1 + \alpha ([\xi_j + (1 - \xi_j)\sigma^{-1}] U_j) \frac{1}{H} \nabla U_j \right\}.$$

Spatially integrating twice gives

$$v u^1 = \sum_{j=1}^N \chi_j(x) \left\{ d_j + H \xi_j c_j + \frac{H^2}{6} [\xi_j^3 + (1 - \xi_j)^3 \sigma^{-1}] g_j^1 + \frac{\alpha H}{6} ([\xi_j^3 + (1 - \xi_j)^3 \sigma^{-1}] U_j) \nabla U_j \right\}.$$

- The inter-element continuity condition (13a) requires that $u^n(X_j, \vec{U}) = 0$ for $n = 1, 2, 3, \dots$, because $u^0(X_j, \vec{U}) = U_j = u(X_j, \vec{U})$. Hence, we solve for d_j at $\xi_j = 0$ and c_j at $\xi_j = 1$, giving

$$\begin{aligned} v u^1 &= \sum_{j=1}^N \chi_j(x) \left\{ \frac{H^2}{6} [\xi_j^3 + (1 - \xi_j)^3 \sigma^{-1} - \xi_j \nabla - \sigma^{-1}] g_j^1 \right. \\ &\quad \left. + \frac{\alpha H}{6} ([\xi_j^3 + (1 - \xi_j)^3 \sigma^{-1} - \xi_j \nabla - \sigma^{-1}] U_j) \nabla U_j \right\} \\ &= \sum_{j=1}^N \chi_j(x) \left\{ \frac{H^2}{6} \mathcal{I}_1 g_j^1 + \frac{\alpha H}{6} (\mathcal{I}_1 U_j) \nabla U_j \right\}, \end{aligned} \quad (28)$$

where it is convenient to introduce interpolation operators $\mathcal{I}_0(\xi_j) := \xi_j + (1 - \xi_j)\sigma^{-1}$ and $\mathcal{I}_1(\xi_j) := \xi_j^3 + (1 - \xi_j)^3 \sigma^{-1} - \xi_j \nabla - \sigma^{-1}$ (observe that $\mathcal{I}_1'' = 6\mathcal{I}_0/H^2$).

- The inter-element smoothness condition (13b) determines the value of g_j^1 . Substitute u^1 from (28) into (13b) and we require

$$-\frac{v\gamma}{H} \delta^2 U_j = -H \left(1 + \frac{1}{6} \delta^2 \right) g_j^1 - \frac{\alpha}{3} (U_j \mu \delta U_j + \mu \delta U_j^2).$$

For this to be satisfied we set

$$g_j^1 = S \left[\frac{\nu\gamma}{H^2} \delta^2 U_j - \frac{\alpha}{3H} U_j \mu \delta U_j - \frac{\alpha}{3H} \mu \delta U_j^2 \right], \quad (29)$$

where nonlocal operator $S := (1 + \delta^2/6)^{-1}$.

Combining these with the initial approximation gives the slow manifold and evolution thereon as

$$u = \sum_{j=1}^N \chi_j(x) \left\{ \mathcal{I}_0 U_j + \frac{H^2}{6\nu} \mathcal{I}_1 g_j^1 + \frac{\alpha H}{6\nu} \mathcal{I}_1 U_j \nabla U_j \right\} + \mathcal{O}(\varepsilon^2), \quad (30a)$$

$$\dot{U}_j = S \left[\frac{\nu\gamma}{H^2} \delta^2 U_j - \frac{\alpha}{3H} U_j \mu \delta U_j - \frac{\alpha}{3H} \mu \delta U_j^2 \right] + \mathcal{O}(\varepsilon^2). \quad (30b)$$

This slow manifold discretisation (30b) is discussed as (6) in the Introduction.

Connection to a cubic spline An intriguing property of the operator $S = (1 + \delta^2/6)^{-1} = 6(\sigma + 4 + \sigma^{-1})^{-1}$ is that it is precisely the operator found in constructing a cubic spline interpolation through equi-spaced data. For example, if the general cubic spline for the j th interval is specified as $S_j(x) = a_j H^3 \xi_j^3/6 + b_j H^2 \xi_j^2/2 + c_j H \xi_j + d_j$, then its second derivative at the left-hand end of the interval is $b_j = S \delta^2 d_j/H^2$, and the corresponding first and third derivatives by $c_j = \nabla \sigma d_j/H - H(2 + \sigma)b_j/6$ and $a_j = \nabla \sigma b_j/H$, respectively. As $d_j = U_{j-1}$ in our example, comparison with the first-order approximation derived above reveals that the holistic approach ensures a cubic spline approximation when $\alpha = 0$ and $\gamma = 1$.

Higher order approximations Higher order terms in the asymptotic series for the slow manifold field u may be systematically computed by iteratively solving equation (27) after having first computed \bar{g}^n (as implemented in the computer algebra code of the Ancillary Material, Appendix A). Such higher-order terms for the field u provide subgrid structures tailored to, and informed by, the dynamics of the PDE, instead of subgrid structures assumed and imposed as in other methodologies.

The solvability condition determines \bar{g}^n [13], namely that the right-hand side of equation (27) must be orthogonal to the null-space of the adjoint of $\nu \partial^2/\partial x^2$ on \bar{X} . Since the operator is self-adjoint, we isolate the boundary between the j th and $(j+1)$ th intervals with the triangular finite-element

$$\hat{v}_0 = \chi_j(x) \xi_j + \chi_{j+1}(x) (1 - \xi_{j+1}), \quad (31)$$

which satisfies both the continuity condition (13a) and the smoothness condition (13b) (for $\gamma = 0$). Now, recall that $u^n(X_j, \bar{U}) = 0$ for $n \geq 1$, and hence $[\nu u_x^n]_j = 0$ for $n \geq 2$. Thus, taking the inner product of equation (27) with \hat{v}_0 gives rise to the solvability condition

$$HS^{-1} g_j^n - \left(\mathcal{R}(u^{(n-1)}, \bar{g}^{(n-1)}), \hat{v}_0 \right) = 0 \quad \text{for } n = 2, 3, \dots \quad (32)$$

The higher order advection terms in α and the interactions between α and γ rapidly become more complex. For example, the $\gamma\alpha$ -terms are

$$\begin{aligned} g_j^2 = & \frac{1}{H} \left\{ -\frac{1}{10} S (U_j S \mu \delta U_j) - \frac{1}{6} S (U_j \mu \delta U_j) + \frac{1}{10} S (S U_j \mu \delta U_j) \right. \\ & - \frac{1}{5} S^2 (U_j S \mu \delta U_j) + \frac{13}{30} S^2 (U_j \mu \delta U_j) - \frac{1}{15} S^3 (U_j \mu \delta U_j) \\ & - \frac{1}{15} S^3 \mu \delta U_j^2 + \frac{7}{30} S^2 \mu \delta U_j^2 + \frac{2}{5} U_j S \mu \delta U_j - \frac{11}{30} S \mu \delta U_j^2 \left. \right\} \\ & + \mathcal{O}(\gamma^2, \alpha^2). \end{aligned} \quad (33)$$

Terms purely in the homotopy parameter γ represent smoothing corrections to the diffusion PDE ($\alpha = 0$). Computing to errors $\mathcal{O}(\gamma^4)$, for example, the coarse dynamics of the diffusion PDE is

$$\dot{U}_j = \frac{\nu\gamma}{H^2} S \delta^2 U_j + \frac{\nu\gamma^2}{60H^2} (7 - 2S) S^2 \delta^4 U_j + \frac{\nu\gamma^3}{6300H^2} (94 - 73S + 14S^2) S^3 \delta^6 U_j + \mathcal{O}(\gamma^4). \quad (34)$$

Fig. 6 shows that each additional term in this expansion provides a better approximation to the full continuum dynamics. In particular, since $S = (1 + \frac{1}{6}\delta^2)^{-1} \sim 1 - \frac{1}{6}\delta^2 + \frac{1}{36}\delta^4 + \dots$, then the first term of equation (34) gives $S \delta^2 u = H^2 u_{xx} + \mathcal{O}H^4$ from the relevant Taylor series expansion. Further, the addition of the second term (evaluated at $\gamma = 1$) gives $(1 - \frac{1}{12}\delta^2) \delta^2 u = H^2 u_{xx} + \mathcal{O}H^6$, and the addition of the third term gives $(1 - \frac{1}{12}\delta^2 + \frac{1}{90}\delta^4) \delta^2 u = H^2 u_{xx} + \mathcal{O}H^8$.

Further, observe that $S \mu \delta u \sim (1 - \frac{1}{6}\delta^2) \mu \delta u = H u_x + \mathcal{O}H^5$; hence, the conservative term in equation (29) (for $\alpha > 0$) is of a higher order approximation than the advective term, and the latter will require extra corrective terms to provide the same order of accuracy, as demonstrated by the $\gamma\alpha$ -terms of equation (33).

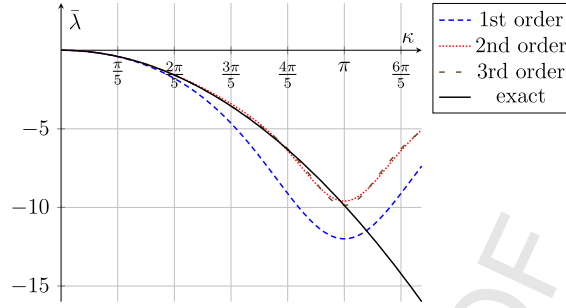


Fig. 6. The non-dimensionalised spectrum ($\bar{\lambda} = \lambda H^2/\nu$ versus $\kappa = kH$) of the diffusion equation ($\alpha = 0$) for the mode $\tilde{u}(x, t) = e^{\lambda t + i k x}$, contrasting the continuum dynamics against successive discrete, holistic approximations (for $\gamma = 1$).

4.2. Dynamical stability of the discretisation

In principle, a slow manifold discretisation is an exact closure of the original PDE, and so exactly shares the same stability. However, in practice we almost always construct and use a truncated order approximation to the slow manifold. Consequently, although we expect our resolution of subgrid structures to improve the correspondence between PDE and discretisation, the stability on an approximate slow manifold is not guaranteed and so needs further consideration.

To algebraically investigate the stability of discretisations to Burgers' PDE (4), we start by considering a mostly undisturbed system where $U_j = 0$ at all grid-points except for M adjacent, internal points. For example, for $M = 2$ it suffices to choose $N = M + 1 = 3$ intervals with outer points fixed at $U_0 = U_N = 0$. Hence, with the transformation $U_j = \frac{\nu}{\alpha H} V_j$, the mixture model (5) reduces to

$$\begin{aligned} \frac{H^2}{\nu} \dot{V}_1 &= -2V_1 + V_2 - \frac{(1-\theta)}{2} V_1 V_2 - \frac{\theta}{4} V_2^2, \\ \frac{H^2}{\nu} \dot{V}_2 &= V_1 - 2V_2 + \frac{(1-\theta)}{2} V_1 V_2 + \frac{\theta}{4} V_1^2. \end{aligned}$$

This reduced system has a stable critical point at $V_1 = V_2 = 0$ with non-dimensionalised eigenvalues $\bar{\lambda} = \frac{H^2}{\nu} \lambda = -1, -3$, and an unstable critical point at $V_1 = -V_2 = \frac{12}{2-3\theta}$ with eigenvalues $\bar{\lambda} = \frac{2}{2-3\theta} \left(\frac{1-\theta}{2} - \frac{9\theta}{4} \right)$. Observe that the unstable point is removed to infinity when $\theta = \frac{2}{3}$. This is exactly the critical value predicted by [9] to be necessary (but not always sufficient) for numerical stability of the mixture model with $\nu = 0$ and $\alpha = 1$. Consequently, the corresponding reduction of the holistic model (6), namely

$$\begin{aligned} \frac{H^2}{\nu} \dot{V}_1 &= -4V_1 + \frac{11}{4} V_2 - \frac{1}{12} V_1^2 - \frac{3}{8} V_1 V_2 - \frac{7}{24} V_2^2, \\ \frac{H^2}{\nu} \dot{V}_2 &= \frac{11}{4} V_1 - 4V_2 + \frac{7}{24} V_1^2 + \frac{3}{8} V_1 V_2 + \frac{1}{12} V_2^2, \end{aligned}$$

is unconditionally stable with critical point at $V_1 = V_2 = 0$ and eigenvalues $\bar{\lambda} = -\frac{5}{4}, -\frac{27}{4}$.

Similarly, for $M = 3$ consecutive points the mixture model (5) reduces to

$$\begin{aligned} \frac{H^2}{\nu} \dot{V}_1 &= -2V_1 + V_2 - \frac{(1-\theta)}{2} V_1 V_2 - \frac{\theta}{4} V_2^2, \\ \frac{H^2}{\nu} \dot{V}_2 &= V_1 - 2V_2 + V_3 - \frac{(1-\theta)}{2} V_2 (V_3 - V_1) - \frac{\theta}{4} (V_3^2 - V_1^2), \\ \frac{H^2}{\nu} \dot{V}_3 &= V_2 - 2V_3 + \frac{(1-\theta)}{2} V_2 V_3 + \frac{\theta}{4} V_2^2. \end{aligned}$$

Substitution of $V_1 = aV_2$ and $V_3 = bV_2$ then leads to

$$V_1 = \frac{\mu(4-\mu\theta)}{8+2\mu(1-\theta)}, \quad V_2 = \mu, \quad V_3 = \frac{\mu(4+\mu\theta)}{8-2\mu(1-\theta)}, \quad (35)$$

where μ satisfies

$$\mu[\theta(1-\theta)(\theta^2-3\theta+1)\mu^4 + 16(2\theta^2-4\theta+1)\mu^2 - 256] = 0. \quad (36)$$

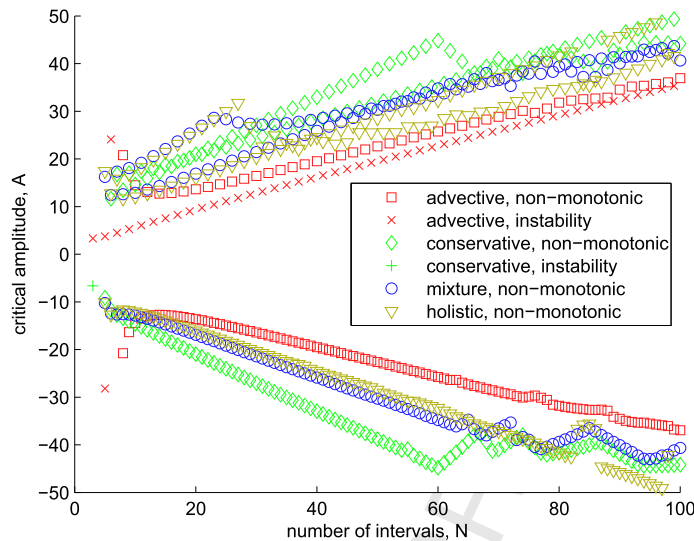


Fig. 7. Stability of numerical integration of Burgers' PDE, with each run starting from $u(x, 0) = A \sin x$. Critical values of A are found for which the numerical solution becomes either unstable (detected when $|u| > 1000$) or non-monotonic. The holistic model is contrasted with the general mixture model for $\theta = 0$ (advective), $\theta = 1$ (conservative) and $\theta = \frac{2}{3}$ (mixture).

The trivial critical point corresponding to $\mu = 0$ is unconditionally stable. Observe that the coefficient of μ^4 vanishes at $\theta = 0, 1$ and $\theta_c = \frac{3-\sqrt{5}}{2}$, and that the resulting quadratic equation only possesses real roots $\mu = \pm 4$ for $\theta = 0$ (the purely advective model). However, the critical point (35) is removed to infinity at exactly these roots, and so there are no unstable critical points when the μ^4 -term vanishes. In general, a pair of unstable critical points arise only when $0 < \theta < \theta_c$. This unstable regime does not include the holistic parameter value of $\theta = \frac{2}{3}$.

Turning now to numerical simulation, we use a 2π -periodic domain with $\nu = 1$ and $\alpha = 1$ for convenience. The initial field $u(x, 0) = A \sin x$ is integrated at the $N + 1$ grid-points $X_j = Hj$ for all $j \in \mathbb{J}$, with spacing $H = \frac{2\pi}{N}$. All time integration for this article was computed with MATLAB's `ode15s`. The integration is performed for a maximum duration of $T = 10$, but ceases early at the first sign of either: an instability, detected when $|U_j| > 1000$ (denoted by 'x'); or a non-monotonic irregularity (denoted by '+'). For each number N of discretised intervals, a search is made over values of A , both positive and negative, for which instability or irregularity first occurs, as plotted in Fig. 7.

The numerical results support the above theoretical results, namely that for $N = 3$ intervals ($M = 2$ internal points), only the advective model ($\theta = 0$) and conservative model ($\theta = 1$) display instabilities, and that for $N = 4$ none of the simulated models (for $\theta = 0$ and $\theta > \theta_c$) show instability, nor irregularity. Overall, the advective model continues to display instability for odd N , and shows irregularity for even N , both of which occur for lower $|A|$ than the other models. In contrast, the other models are susceptible to irregularity but not instability, with the critical values of amplitude A roughly inversely proportional to the number N of intervals, and thus proportional to the grid-spacing H . None of the conservative, mixture or holistic models inherently outperforms the others in this measure. But an advantage of the holistic approach is the rigorous theoretical support, the automatic smooth cubic spline approximation to the out-of-equilibrium subgrid fields, and the automatic derivation of practical sound closures with unambiguous approximation of the spatial derivatives.

5. Conclusion

Holistic discretisation has proved to have a number of attractive properties when applied to the general class of diffusive PDEs described in Section 1. In particular, it empowers centre manifold theory, discussed in Section 3, to use the PDE to inform iterative refinement from an initial approximation to a field $u(x, t)$ whilst incorporating the macroscale dynamics of the relevant PDE. The resulting approximation is a function of the discrete grid values $U_j(t)$, the PDE parameters, and an introduced homotopy parameter γ that controls continuity and smoothness.

The use of a piecewise-linear initial approximation u^0 to u , discussed in Section 3, has been shown to be especially effective in conjunction with the holistic approach. With the inner continuity and smoothness conditions, for instance, the self-adjointness of the diffusion operator \mathcal{L} is preserved under periodic, Dirichlet or Neumann outer boundary conditions. This holds for all $\gamma \in [0, 1]$, although the usual Neumann condition holds exactly only for $\gamma = 1$ and requires modification for $\gamma < 1$ (governed by the chosen smoothness condition). As discussed in the example application of Section 4, also interesting is that with the addition of the first-order holistic correction u^1 , the approximation $u^0 + u^1$ for the diffusion equation ($\alpha = 0$) is an exact cubic spline representation of u in terms of U_j . Notably, this cubic spline is defined in terms of the nonlocal operator S , which appears naturally in the holistic derivation of the coarse dynamics. There remains scope

for research into finding an alternative form of the smoothness condition that would lead to C^n smoothness for \mathcal{O}_Y^{n+1} approximations.

Another useful facet of holistic discretisation is that it eliminates the ambiguity inherent in choosing appropriate discrete approximations to the spatial derivatives in the PDE. Section 4 illustrates that the induced discretisation follows directly from the PDE, as a function of the initial approximation u^0 . Furthermore, at least in the case of Burgers' PDE with a piecewise-linear initial approximation, Section 4.2 indicated that the holistic discretisation automatically favours numerically stable approximations. Indeed, the iterative refinement provided by the centre manifold framework acts to improve the order of approximation of spatial derivatives in terms of the discrete grid-spacing H , as discussed in Section 4. This is somewhat akin to the process of deriving a geometric integration scheme, but applied spatially rather than temporally. It would be interesting to compare the stability of the fully second-order holistic approximation against the mixture model with correspondingly higher-order spatial derivative approximations.

Finally, another active research direction is the extension of piecewise-linear holistic discretisation to two or more spatial dimensions, analogous to the results of [27]. In general, there is exciting scope for exploring many more applications of this new approach.

Acknowledgements

AJR thanks the Australian Research Council for partial support of this project through grant DP150102385.

Appendix A. Ancillary material: computer algebra

The following computer algebra code constructs successive slow manifold approximations to Burgers' PDE (4). It is written in the freely available language Reduce.¹

```

1  %% Key:
2  %% hh := H = X_j - X_{j-1}
3  %% xi := xi_j = (x - X_{j-1}) / H
4  %% uu = U_j
5  %% p := E^+ = sigma, right-shift
6  %% m := E^- = sigma^{-1}, left-shift
7  %% d2 := delta^2 = p + m - 2
8  %% ss := S = (1 + delta^2/6)^{-1}
9  %% md := mu*delta = (p - m)/2
10
11 on div; off allfac; on revpri;
12 factor hh, alpha, gamma, nu;
13
14 depend xi, j;
15 depend uu, j, t;
16 depend gg, j;
17
18 operator p, m, d2, md, ss;
19 linear p, m, d2, md, ss;
20
21 %% Expansions:
22 let p(~z,j) => z + md(z,j) + d2(z,j)/2,
23     m(~z,j) => z - md(z,j) + d2(z,j)/2;
24
25 %% Independence:
26 let md(1,j) => 0,
27     d2(1,j) => 0,
28     ss(1,j) => 1;
29
30 %% Canonical orderings:
31 let md(ss(~z,j),j) => ss(md(z,j),j);
32 let d2(ss(~z,j),j) => ss(d2(z,j),j);
33 let md(d2(~z,j),j) => d2(md(z,j),j);
34
35 %% Invariants:
36 % From direct expansion, for p(m(z)) = m(p(z)) = z:
37 let md(md(~z,j),j) => d2(z,j) + d2(d2(z,j),j)/4;

```

¹ <http://www.reduce-algebra.com>.

```

1  38 % Next follows from definition of S:
2  39 let ss(d2(~z,j),j) => 6*(z-ss(z,j));
3  40 % Next follows from expanding mu*delta z^2:
4  41 let d2(~y,j)*md(~z,j) => md(z^2,j) - 2*z*md(z,j) when y=z;
5  42 % Next two follow from p(y*m(z)) = p(y)*z and m(y*p(z)) = m(y)*z:
6  43 let md(~y*md(~z,j),j) =>
7  44   1/2*(1/2*d2(y*d2(z,j),j) + y*d2(z,j) - z*d2(y,j) + d2(y*z,j));
8  45 let md(~y*d2(~z,j),j) =>
9  46   d2(y*md(z,j),j) + 2*(y*md(z,j) + z*md(y,j) - md(y*z,j));
10 47 % Next follows from either m(z)^2 = m(z^2) or p(z)^2 = p(z^2):
11 48 let md(~z,j)^2 => 1/2*d2(z^2,j) - 1/4*d2(z,j)^2 - z*d2(z,j);
12 49
13 50 % Temporo-spatial composition:
14 51 let df(uu,t) => gg;
15 52 operator !~f;
16 53 let df(~f(~z,j),t) => f(df(z,t),j);
17 54 let df(~z,x) => df(z,xi)/hh;
18 55 let df(~z,x,2) => df(z,xi,2)/hh^2;
19 56
20 57 % Initiate approximations:
21 58 u0 := xi*uu + (1-xi)*m(uu,j);
22 59 u := u0;
23 60 g := 0;
24 61
25 62 % Constrain higher-order terms (adjust as desired):
26 63 let gamma^2 => 0, alpha^2 => 0;
27 64 for iter := 1:3 do begin
28 65
29 66 % Compute internal boundary conditions:
30 67 amp := sub(xi=1,u) - uu; % u|X_j = U_j
31 68 cty := sub(xi=0,p(u,j)) - sub(xi=1,u); % [u]_j = 0
32 69 ux := df(u,x)$
33 70 jmp := sub(xi=0,p(ux,j)) - sub(xi=1,ux)
34 71   - (1-gamma)*sub(xi=1,d2(u,j))/hh; % [u']_j = (1-gamma)/H*delta^2 U_j
35 72 pde := -sub(gg=g,df(u,t)) + nu*df(ux,x) - alpha*u*ux;
36 73
37 74 % Satisfy solvability condition, <v0,pde> = 0, where
38 75 % v0 := xi + p(1-xi,j), to obtain g_n;
39 76 % ensure internal boundary conditions are met.
40 77 % (Note: Use temporary variables to avoid weird error in integration):
41 78 pde_xi := pde*xi$
42 79 pde_lmx := (1-xi)*pde$
43 80 slv := (int(pde_xi,xi,0,1) + p(int(pde_lmx,xi,0,1),j))*hh + nu*jmp;
44 81 % Update g from error in solvability:
45 82 gn := ss(slv,j)/hh;
46 83 % Update u by solving pde = 0 for u := u + u_n:
47 84 tn := xi*gn + (1-xi)*m(gn,j) - pde$
48 85 un := hh^2*int(int(tn,xi),xi)/nu$
49 86 % Impose integration constants to satisfy u_n|X_{j-1} = 0, u_n|X_j = 0:
50 87 un := un - sub(xi=1,un)*xi;
51 88 % Update iteration:
52 89 u := u + un;
53 90 g := g + gn;
54 91
55 92 end;
56 93
57 94 % Compute internal boundary conditions:
58 95 amp := sub(xi=1,u) - uu; % u|X_j = U_j
59 96 cty := sub(xi=0,p(u,j)) - sub(xi=1,u); % [u]_j = 0
60 97 ux := df(u,x)$
61 98 jmp := sub(xi=0,p(ux,j)) - sub(xi=1,ux)
62 99   - (1-gamma)*sub(xi=1,d2(u,j))/hh; % [u']_j = (1-gamma)/H*delta^2 U_j
100 100 pde := -sub(gg=g,df(u,t)) + nu*df(ux,x) - alpha*u*ux;
101 101
102 102 % Apply further invariants for advection terms:
103 103 let ss(md(ss(uu,j)*uu,j),j) =>

```

```

1 104      ss(ss(md(uu,j),j)*uu,j)
2 105      - 1/2*ss(md(uu,j)*ss(uu,j),j)
3 106      - 3/2*ss(md(uu,j),j)*uu
4 107      + 3/2*ss(md(uu^2,j),j);
5 108
6 109      let ss(md(uu,j)*ss(md(uu,j),j),j) =>
7 110      18*uu**2
8 111      - 9*ss(uu,j)*uu
9 112      + 6*ss(ss(uu,j)*uu,j)
10 113      - 3/2*ss(d2(uu,j)*uu,j)
11 114      - 2*ss(md(ss(md(uu,j),j)*uu,j),j)
12 115      - 15*ss(uu**2,j);
13 116
14 117      let ss(d2(uu,j)*ss(md(uu,j),j),j) =>
15 118      - 6*ss(md(uu,j)*uu,j)
16 119      + 3*ss(md(uu,j)*ss(uu,j),j)
17 120      - 3*ss(md(uu,j),j)*uu
18 121      + 3*ss(md(uu**2,j),j);
19 122
20 123      let ss(md(ss(md(uu,j),j)*uu,j),j) =>
21 124      - 6*ss(uu,j)*uu
22 125      + 3*ss(ss(uu,j)*uu,j)
23 126      - 1/2*ss(d2(uu,j)*ss(uu,j),j)
24 127      - 6*ss(uu**2,j)
25 128      + 9*uu**2;
26 129
27 130      % Check internal boundary conditions are satisfied (all zero):
28 131      amp;
29 132      cty;
30 133      jmp;
31 134      pde;
32 135
33 136      end;

```

References

- [1] B. Aulbach, T. Wanner, Integral manifolds for Caratheodory type differential equations in Banach spaces, in: B. Aulbach, F. Colonius (Eds.), Six Lectures on Dynamical Systems, World Scientific, Singapore, 1996, pp. 45–119.
- [2] B. Aulbach, T. Wanner, Invariant foliations for Caratheodory type differential equations in Banach spaces, in: V. Lakshmikantham, A.A. Martynyuk (Eds.), Advances of Stability Theory at the End of XX Century, Gordon & Breach Publishers, 1999, <http://citeseerx.ist.psu.edu/viewdoc/download?doi=10.1.1.45.5229&rep=rep1&type=pdf>.
- [3] B. Aulbach, T. Wanner, The Hartman–Grobman theorem for Caratheodory-type differential equations in Banach spaces, Nonlinear Anal. 40 (2000) 91–104, [https://doi.org/10.1016/S0362-546X\(00\)85006-3](https://doi.org/10.1016/S0362-546X(00)85006-3).
- [4] J.E. Bunder, A.J. Roberts, Resolution of subgrid microscale interactions enhances the discretisation of nonautonomous partial differential equations, Appl. Math. Comput. 304 (2017) 164–179. doi: 10.1016/j.amc.2017.01.056.
- [5] J. Carr, Applications of Centre Manifold Theory, Appl. Math. Sci., vol. 35, Springer-Verlag, 1981, <http://books.google.com.au/books?id=93BdN7btys0C>.
- [6] S.M. Cox, A.J. Roberts, Initialisation and the Quasi-Geostrophic Slow Manifold, Technical report, 1994, <http://arXiv.org/abs/nlin.CD/0303011>, <http://arXiv.org/abs/nlin.CD/0303011>.
- [7] S.M. Cox, A.J. Roberts, Initial conditions for models of dynamical systems, Physica D 85 (1995) 126–141.
- [8] S. Dhawan, S. Kapoor, S. Kumar, S. Rawat, Contemporary review of techniques for the solution of nonlinear Burgers equation, J. Comput. Sci. 3 (5) (2012) 405–419.
- [9] B. Fornberg, On the instability of the leap-frog and Crank–Nicolson approximations of a nonlinear partial differential equation, Math. Comput. 27 (1973) 45–57.
- [10] J.F. Grcar, John von Neumann's analysis of Gaussian elimination and the origins of modern numerical analysis, SIAM Rev. 53 (4) (2011) 607–682, <http://www.siam.org/journals/sirev/53-4/73471.html>.
- [11] M. Haragus, G. Iooss, Local Bifurcations, Center Manifolds, and Normal Forms in Infinite-Dimensional Dynamical Systems, Springer, 2011.
- [12] T.J.R. Hughes, Multiscale phenomena: Green's functions, the Dirichlet-to-Neumann formulation, subgrid scale models, bubbles and the origins of stabilized methods, Comput. Methods Appl. Mech. Eng. 127 (1995) 387–401.
- [13] G.A. Jarrad, Perturbations, Chaos and Waves, PhD thesis, University of South Australia, 2001.
- [14] I.G. Kevrekidis, G. Samaey, Equation-free multiscale computation: algorithms and applications, Annu. Rev. Phys. Chem. 60 (2009) 321–344, <https://doi.org/10.1146/annurev.physchem.59.032607.093610>.
- [15] E.N. Lorenz, V. Krishnamurthy, On the non-existence of a slow manifold, J. Atmos. Sci. 44 (1987) 2940–2950.
- [16] G.N. Mercer, A.J. Roberts, A centre manifold description of contaminant dispersion in channels with varying flow properties, SIAM J. Appl. Math. 50 (1990) 1547–1565, <http://link.aip.org/link/?SMM/50/1547/1>.
- [17] D.P. O'Leary, Scientific Computing with Case Studies, SIAM, Philadelphia, 2008, <http://www.ec-securehost.com/SIAM/OT109.html>.
- [18] C. Potzsche, M. Rasmussen, Taylor approximation of integral manifolds, J. Dyn. Differ. Equ. 18 (2006) 427–460, <https://doi.org/10.1007/s10884-006-9011-8>.
- [19] A.J. Roberts, Appropriate initial conditions for asymptotic descriptions of the long term evolution of dynamical systems, J. Aust. Math. Soc. Ser. B, Appl. Math 31 (1989) 48–75. doi: 10.1017/S0334270000006470

- [20] A.J. Roberts, Low-dimensional modelling of dynamics via computer algebra, *Comput. Phys. Commun.* 100 (1997) 215–230, [https://doi.org/10.1016/S0010-4655\(96\)00162-2](https://doi.org/10.1016/S0010-4655(96)00162-2).
- [21] A.J. Roberts, Holistic discretisation ensures fidelity to Burgers' equation, *Appl. Numer. Math.* 37 (2001) 371–396, [https://doi.org/10.1016/S0168-9274\(00\)00053-2](https://doi.org/10.1016/S0168-9274(00)00053-2), <http://arXiv.org/abs/chao-dyn/9901011>.
- [22] A.J. Roberts, A holistic finite difference approach models linear dynamics consistently, *Math. Comput.* 72 (2003) 247–262, <http://www.ams.org/mcom/2003-72-241/S0025-5718-02-01448-5>.
- [23] A.J. Roberts, Choose interelement coupling to preserve self-adjoint dynamics in multiscale modelling and computation, *Appl. Numer. Math.* 60 (2010) 949–973.
- [24] A.J. Roberts, *Model Emergent Dynamics in Complex Systems*, SIAM, Philadelphia, 2015, <http://bookstore.siam.org/mm20/>.
- [25] A.J. Roberts, Backwards Theory Supports Modelling via Invariant Manifolds for Non-Autonomous Dynamical Systems, Technical report, 2018, <http://arxiv.org/abs/1804.06998>.
- [26] A.J. Roberts, I.G. Kevrekidis, General tooth boundary conditions for equation free modelling, *SIAM J. Sci. Comput.* 29 (4) (2007) 1495–1510, <http://link.aip.org/link/?SCE/29/1495/1>.
- [27] A.J. Roberts, T. MacKenzie, J. Bunder, A dynamical systems approach to simulating macroscale spatial dynamics in multiple dimensions, *J. Eng. Math.* 86 (1) (2014) 175–207, <http://arxiv.org/abs/1103.1187>.
- [28] G. Strang, G. Fix, *An Analysis of the Finite Element Method*, 2nd edn, SIAM, Philadelphia, 2008, <http://bookstore.siam.org/wc08/>.
- [29] D.Z. Turner, K.B. Nakshatrala, K.D. Hjelmstad, A stabilized formulation for the advection–diffusion equation using the Generalized Finite Element Method, *Int. J. Numer. Methods Fluids* 66 (1) (2011) 64–81.
- [30] N.G. van Kampen, Elimination of fast variables, *Phys. Rep.* 124 (1985) 69–160.

Sponsor names

Do not correct this page. Please mark corrections to sponsor names and grant numbers in the main text.



5Q5 Australian Research Council, country=Australia, grants=DP150102385